Stress-Induced Mucosal Layer Disruption Drives Gut Dysbiosis and Depressive-like Behaviors

Courtney Rivet-Noor[1,2,3], Andrea R Merchak[1,2,3], Caroline Render[4], Rebecca M. Beiter[1,2,3], Ryan Brown[1,2,3], Erica Slogar[3], Austin Keeler[5], G. Brett Moreau[6], Sihan Li[2,7], Deniz E. Olgun[8,9], Tobey Mihn Huu Phan[9], Jung-Bum Shin[2,7], Chris Deppmann[5], and Alban Gaultier[1,2].

[1]Center for Brain Immunology and Glia, University of Virginia School of Medicine, Charlottesville, VA 22908, USA. [2]Department of Neuroscience, University of Virginia School of Medicine, Charlottesville, VA 22908, USA. [3]Graduate Program in Neuroscience, University of Virginia School of Medicine, Charlottesville, VA 22908, USA. [4]Undergraduate Department of Global Studies, University of Virginia College of Arts and Sciences, Charlottesville, VA, 22904, USA. [5]Department of Biology, University of Virginia College of Arts and Sciences, Charlottesville, VA, 22904, USA. [6]Division of Infectious Diseases and International Health, Department of Medicine, University of Virginia School of Medicine, Charlottesville, Virginia, USA. [7]Graduate Program in Biochemistry and Molecular Genetics, University of Virginia School of Medicine, Charlottesville, VA 22908, USA. [8]Undergraduate Department of Computer Science, University of Virginia School of Engineering and Applied Science, Charlottesville, VA 22904, USA. [9]Undergraduate Department of Neuroscience, Studies, University of Virginia College of Arts and Sciences, Charlottesville, VA, 22904, USA.

Abstract:

Depression is a common mental health condition with a large social and economic impact. While depression etiology is multifactorial, chronic stress is a well-accepted contributor to disease onset. In addition, depression is associated with altered gut microbial signatures that can be replicated in animal models. While targeted restoration of the microbiome has been shown to reduce depressive-like behaviors in mice, the complexity and diversity of the human microbiome has complicated therapeutic intervention in patients. To circumvent these limitations, there is a critical need for identifying pathways responsible for microbiome dysbiosis. Here, for the first time, we identify the changes in host physiology that induce microbiome dysbiosis. Specifically, we show that a component of mucosal layer, the transmembrane protein mucin 13, can regulate microbiome composition. Using a model of chronic stress to induce behavioral and microbial changes in mice, we show a significant reduction in mucin 13 expression across the intestines that occurs independently of the microbiome. Furthermore, deleting *Muc13* leads to gut dysbiosis, and baseline behavioral changes normally observed after stress exposure. Together, these results validate the hypothesis that mucosal layer disruption is an initiating event in stress-induced dysbiosis and offer mucin 13 as a potential new therapeutic target for microbiome dysbiosis in stress-induced depression. For the first time, our data provide an upstream and conserved target for treating microbiome dysbiosis, a result with sweeping implications for diseases presenting with microbial alterations.

38 **Main:**

39 Depression and anxiety impact millions of people worldwide.[1] Although many treatments
40 exist for these disorders, high rates of treatment-resistant cases remain.[2] While the etiology of
41 depression remains complex, stress is known to be one of the largest contributing factors.[3,4] In
42 addition, stress and depression are both associated with changes in the gut microbiome.[5,6] Gut
43 microbiome dysbiosis is present in depressed patients and conserved in animal models of
44 depression, and has been targeted as a potential treatment for mental health disorders.[7-9]
45 Importantly, modification of the microbiome has been shown to reduce depression symptoms in
46 humans and depressive-like behaviors in mice.[8,10] While promising, efforts to therapeutically
47 manipulate the host microbiome remain inconsistent due to its complexity, unknown microbe-
48 microbe interactions, failure of therapeutic microbes to colonize, microbe resource availability,
49 and host heterogeneity.[7,11,12] To circumvent current microbiome therapeutic limitations, there is
50 a critical need to identify conserved, targetable regulators of the microbiome.

51

52 **Unpredictable Chronic Mild Restraint Stress Drives Anxiety- and Depressive-like Behaviors and**
53 **Modifies the Gut Microbiome Composition:**

54 To investigate the mechanisms of stress-induced microbiome dysbiosis, we used
55 unpredictable chronic mild restraint stress (UCMRS), a model of chronic stress known to induce
56 anxiety- and depressive-like behaviors and alter gut flora (Fig. 1a).[8] After three weeks, mice
57 exposed to UCMRS, but not naïve controls, showed a significant increase in anxiety- like
58 behaviors characterized by an increase in nestlet shredding and decrease in time spent in the
59 open arms of the elevated plus maze (Fig. 1b). Depressive-like behaviors were also detected in

60 the tail suspension, forced swim, and sucrose preference tests (Fig. 1b). In addition to behavioral
61 readouts, levels of murine stress-associated markers were measured in serum by mass
62 spectrometry (Fig. 1c and Ext. Data 1a-g). An increase in murine cortisol levels and a decrease in
63 both serotonin and glutamate were observed, confirming a robust anxiety- and depressive-like
64 phenotype (Fig. 1c and Ext. Data 1a-g).[13,14]

65 We next evaluated stress-induced microbiome composition changes by performing 16S
66 sequencing on fecal DNA from stressed and naïve animals. While we observed no differences in
67 measures of alpha diversity (richness (Fig. 1d) or evenness (Ext. Data 1h)), there were significant
68 differences in beta diversity between naïve and stressed animals. These differences were driven
69 by changes in community composition of several bacterial orders in the stressed group.
70 Specifically, stress drove relative reductions in *Clostridiales*, *Lactobacillales*, and expansion of
71 *Bacteroidales* (Fig. 1f and Ext. Data 1i). Lastly, a random forest model accurately predicted the
72 bacterial orders associated with either baseline or stressed groups, strengthening the link
73 between stress and microbiome dysbiosis (Fig. 1g). Taken together, these results demonstrate
74 that unpredictable chronic mild restraint stress (UCMRS) induces anxiety- and depressive-like
75 behaviors in mice, alters murine stress hormone levels, and changes microbial composition at
76 the bacterial order level.

77

78 **Unpredictable Chronic Mild Restraint Stress Reduces Mucin 13 Expression *In Vivo*:**

79 While it is well accepted that stress can change the microbiome in humans and mice (Fig.
80 1), the mechanisms behind this change are unknown.[7,15-18] Because the mucosal layer, mostly
81 composed of mucins, provides both an anchor point and nutrient reservoir for bacteria, we

82 hypothesized that a change in mucus composition could induce microbiome dysbiosis.[19-21] To test
83 this, we examined mucin RNA expression from individual sections of the intestines in mice
84 exposed to UCMRS and naïve controls (Fig. 2a-c). Of all the mucins tested (*Muc1, 2, 3, 4*, and *13*),
85 we found that mucin 13 was uniquely reduced across intestinal segments (Fig. 2b-c and Ext. Data
86 2a-c). Additionally, we found a similar reduction in mucin 13 in BALB/cJ mice exposed to stress
87 (Ext. Data 2d-e). Taken together, these results suggest that stress induces changes in the mucosal
88 layer in a protein specific manner, and that these changes are conserved across different genetic
89 backgrounds.
90
91 **Mucin 13 Reductions Occur Independently of Stress Hormones and the Microbiome**
92 To understand how stress induces reductions in mucin 13, we began by exploring
93 pathways impacted or driven by stress. First, we tested the direct impact of a stress hormone,
94 hydrocortisone on gut organoids prepared from human and mouse intestinal tissues (Fig. 2d).[22,23]
95 No reductions in mucin 13 expression were observed in either human (Fig. 2e) or mouse (Fig. 2g)
96 organoids. Additionally, we found that none of the mucins tested (*Muc1*, *Muc2*, *Muc3*, *MUC2*,
97 *MUC4*, and *MUC17*) had reductions in expression after treatment (Fig. 2f and h and Ext. Data 2f-
98 i). In addition, mouse organoids also did not downregulate mucin 13 expression after exposure
99 to corticosterone (Ext. Data 2j-m). These results suggest that neither hydrocortisone nor cortisol
100 directly impact the intestinal expression of mucin 13 by gut organoids.
101 In addition, while our central question aimed to understand how stress changes the
102 microbiome, it is possible that changes in the microbiome, a known influencer of the mucus layer,
103 could modulate the expression of mucin 13.[21,24] If true, this would suggest that mucin 13 changes

104 would occur after microbiome dysbiosis in our model. To test this hypothesis, we transferred
105 fecal microbiomes from naïve or stressed mice into mice treated with antibiotics for 2 weeks (Fig.
106 2i). Two weeks post reconstitution, intestinal samples were collected to examine microbiome
107 composition and mucin expression. 16S sequencing revealed that donor samples clustered
108 distinctly from each other (Ext. Data 2n, light blue and dark pink). In addition, recipient mice
109 clustered nearer to their donor sample and separately from each other, demonstrating distinct
110 microbiomes (Ext. Data 2n-o). We next examined RNA expression of mucins from the intestines
111 of these groups. Importantly, no change in mucin 13 expression was detected between groups
112 (Fig. 2j). These data suggest that mucin 13 changes occur independently of and precede
113 microbiome dysbiosis.
114
115 **Mucin 13 Deletion Induces Baseline Behavioral and Microbiome Changes and Lends Mice More**
116 **Susceptible to UCMRS:**
117 Given our data demonstrating that mucin 13 is specifically downregulated in stressed
118 animals, we sought to examine if deleting mucin 13 impacted the microbiome and depressive-
119 and anxiety-like behaviors in mice. Using the *i*-GONAD system, we created a mucin 13 knockout
120 (*Muc13*$^{-/-}$) line by deleting a 475bp region of the gene containing the start codon (Fig. 3a).[25,26]
121 Validation of the knockout line was performed using both qPCR (Fig. 3b-c) and
122 immunofluorescence (Fig. 3d-e). Importantly, no changes were observed in Muc2 at the
123 transcript or protein levels, suggesting that other mucins were not compensating for the loss of
124 *Muc13* (Fig. 3c and f). Together, these data demonstrate successful deletion of mucin 13 in our
125 knockout line.

126 We next sought to understand the impacts of mucin 13 deletion on microbiome
127 composition. We compared 16S sequencing results from fecal samples collected from adult
128 wildtype and *Muc13*$^{-/-}$ animals, separated by genotype at weaning, at baseline and after UCMRS
129 exposure (Fig. 4a). Interestingly, we found that *Muc13*$^{-/-}$ animals clustered distinctly from
130 wildtype controls, suggesting that mucin 13 deletion significantly impacts the composition of the
131 microbiome at baseline (Fig. 4b). In addition, while wildtype controls saw a significant shift in
132 their microbial composition after 1 week of UCMRS, *Muc13*$^{-/-}$ samples remained clustered
133 together (Fig. 4b). This suggests that baseline *Muc13*$^{-/-}$ microbial signatures are not as impacted
134 by stress as baseline signatures in wildtype mice. Importantly, samples from wildtype animals
135 exposed to 1 week of UCMRS shifted towards both groups of the *Muc13*$^{-/-}$ animals, further
136 supporting the idea the *Muc13*$^{-/-}$ animals have microbial signatures that mimics stress-induced
137 microbiome dysbiosis (Fig. 4b). To further understand the similarities between the *Muc13*$^{-/-}$
138 microbiome and UCMRS exposed microbiome, we compared the significantly changed bacterial
139 families between wildtype and *Muc13*$^{-/-}$ animals to the significantly changed bacterial families
140 between baseline animals and animals exposed to 1 week of UCMRS. Of the bacterial families
141 that had significant changes in either group, 69% of those changes overlapped (Fig. 4c). These
142 data further suggest that mucin 13 deletion induces a change in the microbiome that closely
143 mimics the microbiome changes observed after UCMRS exposure.

144 Given the established connection between microbiome changes and mental health, we
145 sought to examine if mucin 13 deletion impacted anxiety- and depressive-like behaviors in mice.[8]
146 Both *Muc13*$^{-/-}$animals and wildtype controls were subjected to the open field, nestlet shred, tail
147 suspension and forced swim tests (Fig. 4a, d-g). Behavior was collected at baseline and after 1

148 week of UCMRS for all animals. Interestingly, at baseline, we observed no differences in anxiety-
149 like behaviors in the open field or nestlet shredding tests between *Muc13*$^{-/-}$ and wildtype controls
150 (Fig. 4d-e, left columns). However, strong depressive-like behaviors were observed in the tail
151 suspension and forced swim tests (Fig. 4f-g, left columns), suggesting *Muc13*$^{-/-}$ mice display innate
152 depressive-, but not anxiety-like, behaviors. In addition, to gain a full picture of the impact of
153 mucin 13 deletion on susceptibility to stress-induced anxiety- and depressive-like behaviors, we
154 subjected wildtype and knockout mice to 1 week of UCMRS. Critically, 1 week of UCMRS
155 exposure is generally considered to be a subclinical model of stress that does not induce
156 behavioral changes in wildtype animals. Thus, we hypothesized that if *Muc13*$^{-/-}$ deletion
157 rendered animals more susceptible to stress, they would exhibit anxiety- and depressive- like
158 behaviors before wildtype animals.[27] Supporting this hypothesis, *Muc13*$^{-/-}$ animals had
159 significant reductions in the amount of time spent in center in the open field test and significant
160 increases in the amount of nestlet removed in the nestlet shred test compared to baseline after
161 1 week of UCMRS exposure. These results indicate that 1 week of UCMRS is sufficient to induce
162 anxiety-like phenotypes in *Muc13*$^{-/-}$ animals, but not their wildtype counterparts (Fig. 4d-e,
163 green columns). Logically, in the tail suspension and forced swim tests, we saw no increase in
164 time spent inactive as the *Muc13*$^{-/-}$ already presented with such behaviors at baseline and hit a
165 ceiling effect (Fig. 4f-g, green columns). To complement these classical behavioral assays, we
166 used unbiased artificial intelligence (DeepLabcut) to detect animal poses (Fig. 4h-j and Ext. Data
167 3).[28,29] In this approach, 10-minute videos of mice exploring an open field box were broken down
168 into 25 individual motifs (Fig. 4h). Each motif was characterized and grouped into a behavioral
169 classification (rearing/grooming, turning, etc.) and changes in the percentage of time spent in

170 each behavioral group were quantified between *Muc13*$^{-/-}$ and wildtype animals (Fig. 4h-j).
171 Baseline analysis revealed that of the 25 distinct motifs, 16% were significantly changed between
172 groups (Ext. Data 3a-b), suggesting that, like in classical behavioral assays, distinctions between
173 *Muc13*$^{-/-}$ and wildtype animals are present at baseline. Similarly, the DeepLabCut software was
174 able to detect significant differences between groups after 1 week of UCMRS exposure, with 40%
175 of behavioral motifs being changed between *Muc13*$^{-/-}$ and wildtype controls (Fig. 4i-j). These
176 results support our behavioral findings and demonstrate that mucin 13 deletion is sufficient to
177 induce behavioral changes, including depressive-like behaviors, at baseline and render animals
178 more susceptible to behavioral changes after stress exposure. Taken together, our results show
179 that mucin 13 deletion can drive both microbiome dysbiosis that mirrors stressed microbiomes
180 and depressive-like behaviors at baseline. In addition, deletion of mucin13 allows animals to be
181 more susceptible to stress-induced microbiome changes. These data highlight the critical nature
182 of mucin 13 in maintaining microbiome and behavioral homeostasis.
183
184 **Discussion:**
185 Our work demonstrates that stress induces microbiome changes and anxiety- and
186 depressive-like behaviors in mice. In addition, stress also reduces expression of a key component
187 of the mucosal layer, mucin 13. While the mechanisms behind stress-induced mucin 13
188 reductions are still being investigated, this change in expression likely does not result from direct
189 stress hormone signaling on intestinal cells or changes in the microbiome. Furthermore, we
190 demonstrate that deletion of mucin 13 is sufficient to induce microbiome dysbiosis and
191 behavioral changes that mimic stress-induced phenotypes at baseline. In addition to these

192 baseline changes, mice lacking mucin 13 also are more susceptible to behavioral changes after
193 sub-clinical exposure to unpredictable chronic mild restraint stress.

194 Our results are supported by previously published literature. For example, it is well known
195 that there is a reciprocal relationship between the mucus layer and microbes.[21] In fact, disruption
196 of this critical layer results in sweeping microbiome changes, heightened inflammation, and
197 disease onset, supporting that concept that changes in mucus can impact other systems in the
198 body.[21,30-37] Additionally, stress is known to alter the glycosylation patterns of mucins.[38] As
199 changes in glycosylation are also known to alter the microbiome, the connection between stress
200 and mucin induced microbiome changes is well supported.[39,40] Furthermore, the connection
201 between mucins and depression has also been suggested in the literature. Specifically, single
202 nucleotide polymorphisms (SNPs) in mucin 13 have been identified in GWAS studies of depressed
203 populations.[41-43] In addition, SNPs in O-glycosylation have also been identified in populations with
204 treatment resistant depression.[43,44] Together, these data support our results suggesting that
205 mucin 13 is an important driver of microbiome dysbiosis and depressive-like behaviors in mice.

206 Mechanistically, more work is needed to determine how stress induces reductions in
207 mucin 13 expression. Our results suggest that stress hormones do not act directly on the
208 intestinal epithelium to drive reductions in mucin 13 expression nor does microbiome dysbiosis
209 alter mucin 13 in the intestines. There are many systems in the body impacted by stress that
210 could mediate changes in mucin 13. For example, the immune system has been known to be
211 influenced by stress and can alter the composition of the microbiome and mucosal layer[45,46]. It is
212 possible that stress can influence the immune system in a way that could alter cytokine
213 expression to act on intestinal cells and reduce mucin 13 expression. In addition, vagal tone is

214 strongly impacted by stress and is known to be altered in depression[47]. Hypothetically, alterations
215 of the vagal nerve could reduce mucin 13 expression because of stress exposure. Finally, it is
216 possible that stress alters circadian rhythms to feedback on the intestines and induce mucin 13
217 expression changes. Data suggests that stress and sleep are connected, as stress-induces
218 significant changes in circadian rhythms.[48-50] In addition, changes in circadian rhythms also have
219 known impacts on the intestine by regulating the microbiome, intestinal regeneration, and the
220 intestinal immune system.[51-53] These works suggest that it is possible for stress to disrupt
221 circadian cycles in a way that disrupts other aspects of health.

222 Here, for the first time, we have defined a previously unknown role for an understudied
223 transmembrane mucus protein. Our work provides a foundation for future research studying the
224 role of mucin 13, and other transmembrane mucins, in microbiome and intestinal homeostasis.
225 Furthermore, our results have brought to light a key aspect in stress-induced depression by
226 defining a mechanism by which stress alters the microbiome. We have demonstrated that a
227 transmembrane mucin is specifically, and indirectly regulated by stress in such a way that
228 interfering with its homeostatic expression patterns induces microbiome dysbiosis and
229 depressive-like behaviors in mice. We believe that this change is a critical step in initiating
230 microbiome dysbiosis in stress-induced depression and that mucin 13 may be a targetable
231 upstream mediator of dysbiosis. As mucin 13 is conserved between humans and mice, this
232 protein could be a broadly applicable target to patients with stress-induced depression that
233 present with microbiome dysbiosis. In addition, while directly related to stress-induced
234 depression, our results provide the basis for further research targeting transmembrane mucins

235 as a broadly applicable intervention point for any disease that presents with or is driven by
236 pathogenic microbiome dysbiosis, such as colitis or Parkinson's Disease.[54]
237
238 **Acknowledgements:** Human organoids were generously gifted from the Moore lab at the
239 University of Virginia. The mass spectrometry experiments were performed in the UVA
240 Biomolecular Research Facility Core. The W.M. Keck Biomedical Mass Spectrometry Laboratory
241 is funded by a grant from the University of Virginia's School of Medicine.
242
243 **Contributions:** C.R.N. and A.G. designed the study; C.R.N., A.R.M., C.R., R.M.B., R.B., E.S., A.K.,
244 C.D. and A.G. performed experiments; G.B.M., S.L., D.E.O, T.M.H.P. and J.B.S. performed
245 sequencing and DeepLab cut analysis; C.R.N and A.G. analyzed and wrote the manuscript; A.G.
246 oversaw the project.

247 **Competing Interests:** Authors declare no competing interests.

248 **Funding:** The authors are supported by grants from the NIMH R33 MH108156, the UVA Trans
249 University Microbiome Initiative pilot grant, and the Owens Family Foundation. C.R.N is
250 supported by the UVA Presidential Fellowship in Neuroscience. A.R.M. is supported by the NINDS
251 T32 NS115657
252

253 **Methods**

254 ***Mice:*** C57BL/6j and BALB/cJ mice were purchased from Jackson Laboratories (strain #000664).
255 Mice were bred in-house and kept on a 12-h light/dark schedule. All mice were housed in groups
256 up to unless in a stressed group or separated for fighting. All behavioral interventions were
257 performed between 8 am and 3 pm and animals were sacrificed between 7 am and 1 pm.
258 Experimental and control animals were sacrificed in alternating patterns to ensure proper
259 controls for circadian experiments. All procedures were approved by the University of Virginia
260 ACUC (protocol #3918). All experiments were conducted and reported according to ARRIVE
261 guidelines. Sex and number of animals is reported in each figure. All animals in the manuscript
262 are between 8-16 weeks of age.

263

264 **METHOD DETAILS**

265 ***Stress Experiments and Behavioral Tests:*** Unpredictable Chronic Mild Restraint Stress (UCMRS)
266 experiments and behavioral experiments (the forced swim, tail suspension, sucrose preference,
267 open field, elevated plus maze, and nestlet shred tests) were performed as previously
268 described.[28]

269 ***Stress protocol:*** For UCMRS, all animals were single housed. Mice were exposed to 2
270 hours of restraint stress and one overnight stressor per day. Restraint stress was performed by
271 putting mice into ventilated 50mL conical tubes for 2 hours. Overnight stressors included one of
272 the following: 45-degree cage tilt, wet bedding, or 2x cage change. Wet bedding was performed
273 by wetting standard cage bedding with ~200mL of murine drinking water. 2x cage change

274 included replacing cage bases 2x within 24 hours. 45-degree cage tilt included propping cages up
275 to ~45-degrees overnight.

276 ***Behavioral Tests:*** All testing (with exception to the nestlet shred and sucrose preference
277 tests) was recorded on a Hero Session 5 GoPro and analyzed with Noldus behavioral analysis
278 software.

279 *Nestlet Shred:* Mice were moved into individual cages and allowed to habituate for 1 hour.
280 After 1 hour, a weighed nestlet was placed in the center of the cage. Mice were allowed to
281 interact with the nestlet for 30 min. After 30 min, nestlets were removed and weighed. Before
282 weighing, excess nestlet was stripped from the main piece of nestlet by lightly dragging fingers
283 across each area of the nestlet starting from the center (center up, center left, center right, center
284 down). Once completed, nestlet was flipped and the process was repeated for the corners (center
285 to upper right, center to upper left, center to lower right, center to lower left). Equal pressure
286 was applied to each nestlet. Change in amount shredded and % shredded were calculated from
287 the weighed nestlet values.

288 *Sucrose Preference test:* Mice were housed individually and given 2 water bottles/ cage.
289 One water bottle contained normal drinking water, the other contained 1% sucrose water. Mice
290 had access to the bottles for 3 days. One Day 0, bottles were primed and weighed and put in
291 cages. Day 1: 24 hours later, water bottles were removed from cages and weighed. Once
292 weighed, bottles were replaced, but with swapped positions (i.e.- if sucrose was on the left on
293 Day 0, it was on the right on Day 1). The first night of sucrose preference is considered habituation
294 and the values are not included in analysis. Day 2: 24 hours after replacing water bottles, bottles

295 were weighed and replaced as on day 1. Day 3: 24 hours after replacing water bottles, bottles
296 were removed and weighed for a final time. Sucrose preference was calculated by determining
297 the percentage of each bottle drunk on day 2 and 3 and averaging those values.

298 *Elevated Plus Maze:* Mice were placed on an elevated plus maze apparatus and allowed
299 to explore for 5 minutes. The elevated plus maze was cleaned with 70% ethanol between each
300 run and recorded on a GoPro Hero Session 5 or 8. Files were analyzed with Noldus behavior
301 software.

302 *Open field/DeepLabCut:* Animals were placed into a 14in x 14in box with opaque walls
303 and a clear bottom. Animals were allowed to explore freely for 10 minutes. Hero session 8s were
304 placed ~12in below the box to record animal movements from below. Noldus behavioral
305 software was used to determine if animals were in the perimeter or center of the box. Videos
306 were also used for DeepLabCut analysis. Analysis is described below.

307 ***Mass Spectrometry:*** 25 µL of plasma was extracted using 500 µL of cold acetonitrile
308 followed by vortexing and 10 minutes of centrifugation at 14K rpm. 450 µL of the resulting
309 supernatant was transferred to a clean Eppendorf and dried completely by Speedvac. Each
310 sample was reconstituted with 25 µL of 50% methanol in 0.1% formic acid/water, vortexed and
311 transferred to autosampler vials for analysis by mass spectrometry. Eleven metabolites were
312 quantitated by PRM (parallel reaction monitoring) using a Thermo Orbitrap ID-X mass
313 spectrometer coupled to a Waters BEH C18 column (15 cm x 2.1 mm). Metabolites were eluted
314 with a Vanquish UHPLC system over a 15 min gradient (10 µL injection, 200 µL/min, buffer A –

315 0.1% formic acid in water, buffer B - 0.1% formic acid in methanol). The mass resolution was set
316 to 120K for detection using the transitions outlines in Extended Data 4.
317 Raw data files for samples, blanks and calibration curves were imported into Skyline
318 (https://skyline.ms/project/home/begin.view). Calibration curves were generated with a linear
319 regression. Peak areas for analytes in samples were used for quantification based in the
320 generated calibration curves.
321

322 ***Fecal DNA Extraction and 16S rRNA Gene Sequencing:*** DNA was isolated from fecal pellets using
323 the phenol/chloroform method as described.[8] Samples were then processed with QIAquick PCR
324 purification kit (Qiagen #28106). Full protocol is outlined below:

325 250µL of 0.1 mm zirconia/silica beads (BioSpec #11079101z) were added to a sterile 2 mL
326 screwtop tube (Celltreat #230830). One 4 mm steel ball was added to each tube (BioSpec
327 #11079132ss). 500µL of Buffer A (200 mM TrisHCl, pH 8.0, 200 mM NaCl, 20 mM EDTA) and 210µL
328 of 20% SDS were added to each fecal pellet in a separate 1.7mL tube. Pellets were vortexed and
329 supernatant transferred to the 2mL screwtop tube containing beads. 500µL of
330 Phenol/chloroform/IAA were added to each screwtop tube. Tubes were allowed to beadbeat on
331 high for 4 min at room temperature. Samples were then centrifuge at 12000 rpm for 5 min at
332 4°C. 420µL of the aqueous layer were transferred to a new 1.7mL tube. 100uL of samples were
333 then processed using the Qiagen PCR Purification Kit

334 ***UCMRS experiments:*** The V4 region of the 16S rRNA gene was amplified from each sample using
335 a dual indexing sequencing strategy.[55] Samples were sequenced on the MiSeq platform (Illumina)

336 using the MiSeq Reagent Kit v2 (500 cycles, Illumina #MS102-2003) according to the
337 manufacturer's protocol with modifications found in the Schloss Wet Lab SOP
338 (https://github.com/SchlossLab/MiSeq_WetLab_SOP).
339
340 ***16S Sequence Analysis:*** All processing and analysis of 16S rRNA sequencing data was performed
341 in R (version 4.1.2).[56] Raw sequencing reads were processed for downstream analysis using
342 DADA2 (version 1.22.0).[57] Processing included inspection of raw reads for quality, filtering of low-
343 quality reads, merging of paired reads, and removal of chimeric sequences. Length distribution
344 of non-chimeric sequences was plotted to ensure lengths matched the expected V4 amplicon
345 size. Taxonomy was assigned to amplicon sequence variants (ASVs) by aligning reads with the
346 Silva reference database (version 138.1).[58]
347
348 Microbiota diversity and community composition were analyzed using the packages phyloseq
349 (version 1.38.0), microbiome (version 1.16.0), and vegan (version 2.5.7).[59-61] The packages
350 tidyverse (version 1.3.0), and ggplot2 (version 3.3.5) were used for data organization and
351 visualization.[62,63] Random forest analysis was performed using the and randomForest (version
352 4.6.14), vegan (version 6.0.90), and pROC (version 1.18.0) packages.[64-66]
353
354 Samples were first divided into training (70% of samples, divided equally between Baseline and
355 Stressed samples) and test (30% of samples) sets. The training set was used to tune the “mtry”
356 parameter of the model, while the test set was used to validate model performance. Feature

357 importance was determined using the Gini index, which measures the total decrease in node
358 impurity averaged across all trees.
359
360 ***Microbiome Transfer and Mucin 13 Stress 16S****:* Fecal pellet DNA extraction and 16S sequencing
361 of the V4 region was performed by Zymo according to their protocols.
362
363 ***DeepLabCut:*** Deeplabcut analysis was performed as previously described.[28] Full protocol is
364 outlined below:
365 All machine learning programs and statistical analyses were performed on a computer
366 with an Intel i9-10900KF CPU, a single NVIDIA RTX3080 GPU, and 64GB RAM. Animal pose
367 estimation was performed by using a deep-learning package called DeepLabCut. The detailed
368 mathematical model and network architecture for DeepLabCut was previously published by the
369 Mathis lab [29]. We generated a DeepLabCut convolutional neural network to analyze our open
370 field test videos, which is trained in a supervised manner: 16 manually labeled points were
371 selected as references of transfer learning, including nose, left and right eyes, left and right ears,
372 neck, left and right arm, left and right leg, 3 points on body and 3 points on tail. In total, 15
373 randomly selected videos were used for building a training dataset. Finally, the performance of
374 the neural network is evaluated by human researchers.
375
376 Estimated mouse poses from DeepLabCut were further analyzed by using a package called
377 Variational Animal Motion Embedding (VAME), which classifies animal behavior in an
378 unsupervised manner. VAME was developed by the Pavol Bauer group and the package can be

379 downloaded at https://github.com/LINCellularNeuroscience/VAME [67]. We trained a unique
380 VAME recursive neural network for each experiment, which classifies each frame of the open
381 field test video into 1 of the 25 behavioral motifs. Then, all behavior motifs were annotated and
382 evaluated by human researchers. With annotated frames, we were able to calculate the
383 percentage of time usage of each motif, which is then used for principal component analysis and
384 Kullback-Leibler divergence analysis.

385 ***RNA Extraction and Quantitative PCR:*** For RNA extraction, cultured cells were pelleted, frozen,
386 and lysed. RNA was extracted using the Bioline Isolate II RNA mini kit as per manufacture's
387 protocol (BIO- 52073). RNA was quantified with a Biotek Epoch Microplate Spectrophotometer.
388 Normalized RNA was reverse transcribed to cDNA with either the Bioline SensiFast cDNA
389 Synthesis Kit (BIO-65054) or Applied Sciences High- Capacity cDNA Reverse Transcriptase Kit (43-
390 688-13). cDNA was amplified using the Bioline SensiFast NO- ROX kit (BIO-86020), according to
391 manufacturer's instructions. Results were analyzed with the relative quantity (ΔΔCq) method.
392 Probes used are listed in Extended Data 5.

393 ***Immunofluorescence Staining and Imaging:*** 1cm sections of intestinal samples were harvested
394 and snap frozen in an OCT block (Fisher Scientific #14-373-65). Samples were cut on a cryostat in
395 15μM sections and placed on microscope slides. Tissue was fixed directly on the slides in carnoy's
396 solution (60% Ethanol, 30% Chloroform, and 10% Glacial Acetic Acid) for 10 min at room
397 temperature. Tissue was washed 3x in 1x PBS for 5 min each at room temperature. Antigen
398 retrieval was performed with Tris-EDTA by bringing solution to a boil (~30sec) in a microwave.
399 Slides were washed in 1x PBS 3x for 5 min at room temperature. After final wash, sections were

400 outlined with a hydrophobic pen (Vector Laboratories #H-4000). Samples were blocked for 1 hour
401 at room temperature with 1:200 FC block in TBST (1x TBS + 0.3% Triton X-100) plus 2% Normal
402 Donkey Serum (Jackson ImmunoResearch #017-000-121). Supernatant was removed and
403 samples were blocked with Mouse on Mouse IgG for 1 hour are room temperature (Vector
404 Laboratories #MKB-2213-1) plus 2% Normal Donkey Serum. Supernatant was removed and
405 primary antibodies were added. Samples were stained with 1:1000 Mucin 13 (G-10) (Santa Cruz
406 Biotechnology #sc-390115) and 1:1000 Mucin 2 (GeneTex #GTX100664) overnight at 4 degrees
407 Celsius in blocking solution (1x PBS, 0.5g bovine serum albumin, 0.5% Triton X-100) + 2% normal
408 donkey serum. Control samples were stained in blocking solution + 2% normal donkey serum
409 with mouse IgG (Jackson ImmunoResearch #015-000-003) or rabbit IgG (Jackson
410 ImmunoResearch #011-000-003) diluted to match the primary antibodies. The next day samples
411 were washed 3x in TBST for 5 min at room temperature. Samples were then incubated in
412 secondary antibodies for 3 hours at room temperature in blocking solution + 2% normal donkey
413 serum. Secondary antibodies used were Donkey Anti-Mouse 488 (Jackson ImmunoResearch
414 #715-545-150) and Donkey Anti-Rabbit 647 (Jackson ImmunoResearch #711-605-152).
415 Secondaries were added at 2mg/mL. Samples were then stained with Hoechst (1:700) (Thermo
416 Fisher Scientific #H3570) for 15 min in blocking solution + 2% normal donkey serum. Samples
417 were washed 2x with TBST for 5 min at room temperature. Samples were washed a final time in
418 TBS for 5 min at room temperature. Finally, slides imaged on a Leica Stellaris 5 confocal
419 microscope.

420 ***Organoid Culture:*** Mouse duodenal organoids prepared as previously described.[68] Mice were
421 euthanized with CO_2 according to regulations. Cervical dislocation was performed and small

422 intestine removed. After fat was scraped from the intestine, it was flushed with 1x DPBS-/- (Gibco
423 #14190-144) + 1:100 Pen/Strep (Gibco #15140122). Intestines were flayed open and cut into
424 ~1cm pieces and put into 40mL of 1x DPBS-/- + 1:100 Pen/Strep. Tubes were shaken manually for
425 30 seconds to remove debris. Supernatant was removed and 15mL of fresh DPBS-/- was added
426 to each tube. A 10mL pipette was used to pipette up and down 10 times to remove mucus and
427 additional debris. Supernatant was removed and 20mL of DPBS-/- + 1:100 Pen/Strep +2mM EDTA
428 (Invitrogen 15575-038) was added to each tube. Samples were allowed to incubate at room temp
429 for 30 min on vigorous shaker. Supernatant from samples was removed. 20mL of fresh DPBS-/- +
430 1:100 Pen/Strep was added to each tube. A 10mL pipette was used to pipette up and down 10
431 times and supernatant was filtered into a fresh 50mL tube over a 70μM filter (Celltreat #229483)
432 for fraction 1. Repeat for 4 total fractions. Visualize crypts under a microscope to find the fraction
433 with the purest and most abundant crypt population. Count crypts from chosen fraction. Take
434 enough crypts for 100 crypts/well and spin for 3 min at 300g. Aspirate supernatant and add 50uL
435 matrigel + murine Wnt3a (Peprotech #315-20, 10ug/mL used at 1000x), R-spondin (Peprotech
436 #315-32, 50ug/mL used at 1000x), Noggin (Peprotech #250-38, 50ug/mL used at 1000x), and EGF
437 (Peprotech #315-09, 50ug/mL used at 1000x) per well to crypts. Crypts were plated in 50μL
438 matrigel (Corning # 356237) and grown in intesticult media (Stemcell Technologies # 06005 for
439 mouse and #356237 for human**).** Mouse organoids were treated with either 5ng/mL of
440 hydrocortisone (Sigma # H4001) or 150μg/mL of corticosterone (Cayman Chemical # 16063) for
441 24 hours. Human organoids were treated with 200μM of hydrocortisone (Sigma # H4001) for 12
442 hours.
443

444 ***Mucin-13 Knockout Generation:*** Mucin-13 knockout lines were generated using the iGONAD
445 technique as described using a BTX ECM 830 Electroporation System (Harvard Apparatus).[25,26]).
446 Briefly, the muc13 sequence was taken from the UCSC genome browser, mouse assembly Dec.
447 2011 (GRCm38/mm10), Genomic Sequence (chr16:33,794,037-33,819,927) [69]. Exons 1 and 2
448 including the intervening intron where analyzed with CRISPOR (http://crispor.tefor.net/;
449 Concordet and Haeussler 2018)[70]. Exon 2, containing the protein start sequence, was targeted
450 for excision at these two target sequences + PAM sites. Exon2_protein_start_sequence
451 GCAAGAGCAGCTACCATGAA (AGG) and Exon2_end_of_exon AGTCTCCTTTTGGTGACCGT (GGG).
452 Alt-R S.p. HiFi Cas9 Nuclease, tracrRNA, and crRNA XT for the two target sequences were
453 purchased (IDT). Prior to surgery, the Alt-R CRISPR/Cas9 reagents were prepared according to IDT
454 guidelines: crRNA-XT and tracrRNA were annealed to form the gRNA, then complexed to the S.p
455 HiFi Cas9 nuclease, and then diluted with sterile Opti-MEM with Fast Green FCF to aid
456 visualization.
457
458 Plugged females were anesthetized and maintained with isoflurane ~16 hours after copulation
459 was assumed to have occurred (estimate copulation around midnight thus surgeries were done
460 at 4pm). Anesthesia was confirmed by toe pinch and then eyes were lubricated with Puralube
461 ointment. The lower dorsal skin of the mouse was soaked in betadine followed by two washes
462 with isopropanol. A dorsal incision was made to expose the ovaries, oviduct, and uterine horn.
463 Using a pulled micropipette, ~1.5ul of the CRISPR/Cas9 solution was drawn up and then inject
464 between the infundibulum and ampulla, intraoviductally dispensing the solution slowly to avoid
465 backflow. The oviduct is covered in a wetted, sterile kimwipe and immediately electroporated

466 using a 3-mm platinum tweezertrode electrodes (BTX) delivering 50V for 5ms with 1s interval for
467 8 square-wave pulses using a BTX ECM 830 Electroporation System (Harvard Apparatus). The
468 oviduct is returned to the abdominal cavity and the procedure is repeated on the opposite side
469 oviduct. Once both oviducts have been injected and electroporated the incision was sutured, and
470 the stitches secured with liquid bandage before receiving a postop subcutaneous injection of
471 ketoprofen (5mg/kg of mouse body weight) with subsequent injections for up to five days as
472 needed.
473

474 **QUANTIFICATION AND STATISTICAL ANALYSIS**

475 ***Statistical analysis:*** All statistical analyses-except those associated with DeepLabCut and 16S
476 were performed in GraphPad Prism 9. Analyses involving two groups were performed using a
477 two-tailed T test. If the variances between groups were significantly different, a Welch's
478 correction was applied. Outliers were excluded if they fell more than two standard deviations
479 from the mean. For all analyses, the threshold for significance was at $p < 0.05$. Repeats for each
480 experiment are specified in the figure legend corresponding to the respective panel.

481
482
483
484
485
486

487

488 **References:**

489

490 1 Santomauro, D. F. *et al.* Global prevalence and burden of depressive and anxiety disorders

491 in 204 countries and territories in 2020 due to the COVID-19 pandemic. *The Lancet* **398**,

492 1700-1712, doi:https://doi.org/10.1016/S0140-6736(21)02143-7 (2021).

493 2 Fava, M. Diagnosis and definition of treatment-resistant depression. *Biological Psychiatry*

494 **53**, 649-659, doi:https://doi.org/10.1016/S0006-3223(03)00231-2 (2003).

495 3 Heim, C. & Binder, E. B. Current research trends in early life stress and depression: Review

496 of human studies on sensitive periods, gene–environment interactions, and epigenetics.

497 *Experimental Neurology* **233**, 102-111,

498 doi:https://doi.org/10.1016/j.expneurol.2011.10.032 (2012).

499 4 McGonagle, K. A. & Kessler, R. C. Chronic stress, acute stress, and depressive symptoms.

500 *American Journal of Community Psychology* **18**, 681-706,

501 doi:https://doi.org/10.1007/BF00931237 (1990).

502 5 Lach, G., Schellekens, H., Dinan, T. G. & Cryan, J. F. Anxiety, Depression, and the

503 Microbiome: A Role for Gut Peptides. *Neurotherapeutics : the journal of the American*

504 *Society for Experimental NeuroTherapeutics* **15**, 36-59, doi:10.1007/s13311-017-0585-0

505 (2018).

506 6 Foster, J. A. & McVey Neufeld, K. A. Gut-brain axis: how the microbiome influences anxiety

507 and depression. *Trends in neurosciences* **36**, 305-312, doi:10.1016/j.tins.2013.01.005

508 (2013).

509 7 Berding, K. & Cryan, J. F. Microbiota-targeted interventions for mental health. *Curr Opin*
510 *Psychiatry* **35**, 3-9, doi:10.1097/yco.0000000000000758 (2022).
511 8 Marin, I. A. *et al.* Microbiota alteration is associated with the development of stress-
512 induced despair behavior. *Scientific reports* **7**, 43859-43859, doi:10.1038/srep43859
513 (2017).
514 9 Valles-Colomer, M. *et al.* The neuroactive potential of the human gut microbiota in quality
515 of life and depression. *Nature Microbiology* **4**, 623-632, doi:10.1038/s41564-018-0337-x
516 (2019).
517 10 Tian, P. *et al.* Bifidobacterium breve CCFM1025 attenuates major depression disorder via
518 regulating gut microbiome and tryptophan metabolism: A randomized clinical trial. *Brain,*
519 *behavior, and immunity* **100**, 233-241, doi:https://doi.org/10.1016/j.bbi.2021.11.023
520 (2022).
521 11 Park, S.-Y. *et al.* Strain-level fitness in the gut microbiome is an emergent property of
522 glycans and a single metabolite. *Cell* **185**, 513-529.e521, doi:10.1016/j.cell.2022.01.002
523 (2022).
524 12 Zmora, N. *et al.* Personalized Gut Mucosal Colonization Resistance to Empiric Probiotics
525 Is Associated with Unique Host and Microbiome Features. *Cell* **174**, 1388-1405.e1321,
526 doi:https://doi.org/10.1016/j.cell.2018.08.041 (2018).
527 13 Saldanha, D., Kumar, N., Ryali, V., Srivastava, K. & Pawar, A. A. Serum Serotonin
528 Abnormality in Depression. *Medical Journal Armed Forces India* **65**, 108-112,
529 doi:https://doi.org/10.1016/S0377-1237(09)80120-2 (2009).

530 14 Pfleiderer, B. *et al.* Effective electroconvulsive therapy reverses glutamate/glutamine
531 deficit in the left anterior cingulum of unipolar depressed patients. *Psychiatry Research:*
532 *Neuroimaging* **122**, 185-192, doi:https://doi.org/10.1016/S0925-4927(03)00003-9
533 (2003).
534 15 Bailey, M. T. *et al.* Exposure to a social stressor alters the structure of the intestinal
535 microbiota: implications for stressor-induced immunomodulation. *Brain, behavior, and*
536 *immunity* **25**, 397-407, doi:10.1016/j.bbi.2010.10.023 (2011).
537 16 Bastiaanssen, T. F. S. *et al.* Gutted! Unraveling the Role of the Microbiome in Major
538 Depressive Disorder. *Harv Rev Psychiatry* **28**, 26-39,
539 doi:10.1097/HRP.0000000000000243 (2020).
540 17 Li, N. *et al.* Fecal microbiota transplantation from chronic unpredictable mild stress mice
541 donors affects anxiety-like and depression-like behavior in recipient mice via the gut
542 microbiota-inflammation-brain axis. *Stress* **22**, 592-602,
543 doi:10.1080/10253890.2019.1617267 (2019).
544 18 Karl, J. P. *et al.* Changes in intestinal microbiota composition and metabolism coincide
545 with increased intestinal permeability in young adults under prolonged physiological
546 stress. *American journal of physiology. Gastrointestinal and liver physiology* **312**, G559-
547 g571, doi:10.1152/ajpgi.00066.2017 (2017).
548 19 Pelaseyed, T. & Hansson, G. C. Membrane mucins of the intestine at a glance. *Journal of*
549 *Cell Science* **133**, jcs240929, doi:10.1242/jcs.240929 (2020).
550 20 Johansson, M. E. V. a. H., G. C. *The Mucins* Vol. 2 381-388
551 (2016).

552 21 Hansson, G. C. Mucins and the Microbiome. *Annu Rev Biochem*, doi:10.1146/annurev-
553 biochem-011520-105053 (2020).
554 22 Williams, S. J. *et al.* MUC13, a Novel Human Cell Surface Mucin Expressed by Epithelial
555 and Hemopoietic Cells. *Journal of Biological Chemistry* **276**, 18327-18336,
556 doi:10.1074/jbc.M008850200 (2001).
557 23 Gupta, B. K. *et al.* Functions and regulation of MUC13 mucin in colon cancer cells. *J*
558 *Gastroenterol* **49**, 1378-1391, doi:10.1007/s00535-013-0885-z (2014).
559 24 Sicard, J. F., Le Bihan, G., Vogeleer, P., Jacques, M. & Harel, J. Interactions of Intestinal
560 Bacteria with Components of the Intestinal Mucus. *Frontiers in cellular and infection*
561 *microbiology* **7**, 387, doi:10.3389/fcimb.2017.00387 (2017).
562 25 Gurumurthy, C. B. *et al.* Creation of CRISPR-based germline-genome-engineered mice
563 without ex vivo handling of zygotes by i-GONAD. *Nature Protocols* **14**, 2452-2482,
564 doi:10.1038/s41596-019-0187-x (2019).
565 26 Ohtsuka, M. *et al.* i-GONAD: a robust method for in situ germline genome engineering
566 using CRISPR nucleases. *Genome Biology* **19**, 25, doi:10.1186/s13059-018-1400-x (2018).
567 27 Nollet, M., Guisquet, A.-M. L. & Belzung, C. Models of Depression: Unpredictable Chronic
568 Mild Stress in Mice. *Current protocols in pharmacology* **61**, 5.65.61-65.65.17,
569 doi:https://doi.org/10.1002/0471141755.ph0565s61 (2013).
570 28 Rivet-Noor, C. R. *et al.* Stress-induced despair behavior develops independently of the
571 Ahr-RORγt axis in CD4 + cells. *Scientific reports* **12**, 8594, doi:10.1038/s41598-022-12464-
572 2 (2022).

573 29 Mathis, A. *et al.* DeepLabCut: markerless pose estimation of user-defined body parts with
574 deep learning. *Nature Neuroscience* **21**, 1281-1289, doi:10.1038/s41593-018-0209-y
575 (2018).
576 30 Bergstrom, K. *et al.* Proximal colon–derived O-glycosylated mucus encapsulates and
577 modulates the microbiota. *Science (New York, N.Y.)* **370**, 467-472,
578 doi:10.1126/science.aay7367 (2020).
579 31 Borisova, M. A. *et al.* Mucin-2 knockout is a model of intercellular junction defects,
580 mitochondrial damage and ATP depletion in the intestinal epithelium. *Scientific reports*
581 **10**, 21135, doi:10.1038/s41598-020-78141-4 (2020).
582 32 Wu, M. *et al.* The Dynamic Changes of Gut Microbiota in Muc2 Deficient Mice.
583 *International journal of molecular sciences* **19**, doi:10.3390/ijms19092809 (2018).
584 33 Bergstrom, K. S. *et al.* Muc2 protects against lethal infectious colitis by disassociating
585 pathogenic and commensal bacteria from the colonic mucosa. *PLoS pathogens* **6**,
586 e1000902, doi:10.1371/journal.ppat.1000902 (2010).
587 34 Johansson, M. E., Thomsson, K. A. & Hansson, G. C. Proteomic analyses of the two mucus
588 layers of the colon barrier reveal that their main component, the Muc2 mucin, is strongly
589 bound to the Fcgbp protein. *J Proteome Res* **8**, 3549-3557, doi:10.1021/pr9002504 (2009).
590 35 Johansson, M. E. V. *et al.* The inner of the two Muc2 mucin-dependent mucus layers in
591 colon is devoid of bacteria. *Proceedings of the National Academy of Sciences* **105**, 15064-
592 15069, doi:10.1073/pnas.0803124105 (2008).

36 Van der Sluis, M. *et al.* Muc2-Deficient Mice Spontaneously Develop Colitis, Indicating That MUC2 Is Critical for Colonic Protection. *Gastroenterology* **131**, 117-129, doi:https://doi.org/10.1053/j.gastro.2006.04.020 (2006).

37 Velcich, A. *et al.* Colorectal cancer in mice genetically deficient in the mucin Muc2. *Science (New York, N.Y.)* **295**, 1726-1729, doi:10.1126/science.1069094 (2002).

38 Silva, S. D. *et al.* Stress disrupts intestinal mucus barrier in rats via mucin O-glycosylation shift: prevention by a probiotic treatment. *American Journal of Physiology-Gastrointestinal and Liver Physiology* **307**, G420-G429, doi:10.1152/ajpgi.00290.2013 (2014).

39 Marczynski, M. *et al.* Structural Alterations of Mucins Are Associated with Losses in Functionality. *Biomacromolecules*, doi:10.1021/acs.biomac.1c00073 (2021).

40 Werlang, C., Cárcarmo-Oyarce, G. & Ribbeck, K. Engineering mucus to study and influence the microbiome. *Nature Reviews Materials* **4**, 134-145, doi:10.1038/s41578-018-0079-7 (2019).

41 Ware, E. B. *et al.* Comparative genome-wide association studies of a depressive symptom phenotype in a repeated measures setting by race/ethnicity in the multi-ethnic study of atherosclerosis. *BMC Genetics* **16**, 118, doi:10.1186/s12863-015-0274-0 (2015).

42 Dunn, E. C. *et al.* Genome-wide association study of depressive symptoms in the Hispanic Community Health Study/Study of Latinos. *Journal of psychiatric research* **99**, 167-176, doi:10.1016/j.jpsychires.2017.12.010 (2018).

43 Rivet-Noor, C. & Gaultier, A. The Role of Gut Mucins in the Etiology of Depression. *Front Behav Neurosci* **14**, 592388, doi:10.3389/fnbeh.2020.592388 (2020).

615 44 McClain, L. L. *et al.* Rare variants and biological pathways identified in treatment-
616 refractory depression. *J Neurosci Res* **98**, 1322-1334, doi:10.1002/jnr.24609 (2020).
617 45 Padgett, D. A. & Glaser, R. How stress influences the immune response. *Trends in*
618 *Immunology* **24**, 444-448, doi:https://doi.org/10.1016/S1471-4906(03)00173-X (2003).
619 46 Zhao, Q. & Maynard, C. L. Mucus, commensals, and the immune system. *Gut Microbes*
620 **14**, 2041342, doi:10.1080/19490976.2022.2041342 (2022).
621 47 Breit, S., Kupferberg, A., Rogler, G. & Hasler, G. Vagus Nerve as Modulator of the Brain-
622 Gut Axis in Psychiatric and Inflammatory Disorders. *Frontiers in psychiatry* **9**, 44,
623 doi:10.3389/fpsyt.2018.00044 (2018).
624 48 Ihara, T. *et al.* Intermittent restraint stress induces circadian misalignment in the mouse
625 bladder, leading to nocturia. *Scientific reports* **9**, 10069, doi:10.1038/s41598-019-46517-
626 w (2019).
627 49 Wells, A. M. *et al.* Effects of Chronic Social Defeat Stress on Sleep and Circadian Rhythms
628 Are Mitigated by Kappa-Opioid Receptor Antagonism. *The Journal of Neuroscience* **37**,
629 7656-7668, doi:10.1523/jneurosci.0885-17.2017 (2017).
630 50 Tahara, Y. *et al.* Entrainment of the mouse circadian clock by sub-acute physical and
631 psychological stress. *Scientific reports* **5**, 11417, doi:10.1038/srep11417 (2015).
632 51 Brooks, J. F. *et al.* The microbiota coordinates diurnal rhythms in innate immunity with
633 the circadian clock. *Cell* **184**, 4154-4167.e4112,
634 doi:https://doi.org/10.1016/j.cell.2021.07.001 (2021).

635 52 Stokes, K. *et al.* The Circadian Clock Gene BMAL1 Coordinates Intestinal Regeneration.
636 *Cellular and molecular gastroenterology and hepatology* **4**, 95-114,
637 doi:10.1016/j.jcmgh.2017.03.011 (2017).
638 53 Balakrishnan, A., Tavakkolizadeh, A. & Rhoads, D. B. Circadian clock genes and
639 implications for intestinal nutrient uptake. *The Journal of Nutritional Biochemistry* **23**,
640 417-422, doi:https://doi.org/10.1016/j.jnutbio.2012.01.002 (2012).
641 54 Herath, M., Hosie, S., Bornstein, J. C., Franks, A. E. & Hill-Yardin, E. L. The Role of the
642 Gastrointestinal Mucus System in Intestinal Homeostasis: Implications for Neurological
643 Disorders. *Frontiers in cellular and infection microbiology* **10**,
644 doi:10.3389/fcimb.2020.00248 (2020).
645 55 Kozich, J. J., Westcott, S. L., Baxter, N. T., Highlander, S. K. & Schloss, P. D. Development
646 of a dual-index sequencing strategy and curation pipeline for analyzing amplicon
647 sequence data on the MiSeq Illumina sequencing platform. *Applied and environmental*
648 *microbiology* **79**, 5112-5120, doi:10.1128/aem.01043-13 (2013).
649 56 Team, R. C. R: A language and environment for statistical computing. R Foundation for
650 Statistical Computing. doi:https://www.R-project.org/. (2021).
651 57 Callahan, B. J. *et al.* DADA2: High-resolution sample inference from Illumina amplicon
652 data. *Nat Methods* **13**, 581-583, doi:10.1038/nmeth.3869 (2016).
653 58 Quast, C. *et al.* The SILVA ribosomal RNA gene database project: improved data processing
654 and web-based tools. *Nucleic Acids Res* **41**, D590-596, doi:10.1093/nar/gks1219 (2013).
655 59 Jari Oksanen, F. G. B., Michael Friendly, Roeland Kindt, Pierre Legendre, Dan McGlinn,
656 Peter R. & Minchin, R. B. O. H., Gavin L. Simpson, Peter Solymos, M. Henry H. Stevens,

657 Eduard Szoecs and Helene Wagner. vegan: Community Ecology Package. R package
658 version 2.5-7. doi:https://CRAN.R-project.org/package=vegan
659 (2020).
660 60 McMurdie, P. J. & Holmes, S. phyloseq: An R Package for Reproducible Interactive Analysis
661 and Graphics of Microbiome Census Data. *PloS one* **8**, e61217,
662 doi:10.1371/journal.pone.0061217 (2013).
663 61 Leo Lahti, F. G. M. E., Sudarshan Shetty, Tuomas Borman, Domenick J. Braccia, Ruizhu
664 Huang, Hector Corrada Bravo. Microbiome R package. doi:http://microbiome.github.io.
665 62 Hadley Wickham, M. A., Jennifer Bryan, Winston Cheng, Lucy D'Agostino, Romain
666 François, Garrett Grolemund, Alex Hayes, Lionel Henry, Max Kuhn, Thomas Lin Pedersen.
667 Welcome to the Tidyverse. *Journal of Open Source Software* **4**, 1686,
668 doi:https://doi.org/10.21105/joss.01686 (2019).
669 63 Wickham, H. *ggplot2: Elegant Graphics for Data Analysis.* . (Springer-Verlag 2016).
670 64 Robin, X. *et al.* pROC: an open-source package for R and S+ to analyze and compare ROC
671 curves. *BMC Bioinformatics* **12**, 77, doi:10.1186/1471-2105-12-77 (2011).
672 65 Classification and regression by randomForest (R news 2, 2002).
673 66 Kuhn, M. caret: Classification and Regression Training. *R package version 6.0-90* (2021).
674 67 Luxem, K., Fuhrmann, F., Kürsch, J., Remy, S. & Bauer, P. Identifying Behavioral Structure
675 from Deep Variational Embeddings of Animal Motion. *bioRxiv*, 2020.2005.2014.095430,
676 doi:10.1101/2020.05.14.095430 (2020).
677 68 Sato, T. *et al.* Single Lgr5 stem cells build crypt-villus structures in vitro without a
678 mesenchymal niche. *Nature* **459**, 262-265, doi:10.1038/nature07935 (2009).

679 69 Kent, W. J. *et al.* The human genome browser at UCSC. *Genome Res* **12**, 996-1006,
680 doi:10.1101/gr.229102 (2002).
681 70 Concordet, J.-P. & Haeussler, M. CRISPOR: intuitive guide selection for CRISPR/Cas9
682 genome editing experiments and screens. *Nucleic Acids Research* **46**, W242-W245,
683 doi:10.1093/nar/gky354 (2018).
684
685

686 **MAIN FIGURES:**

687

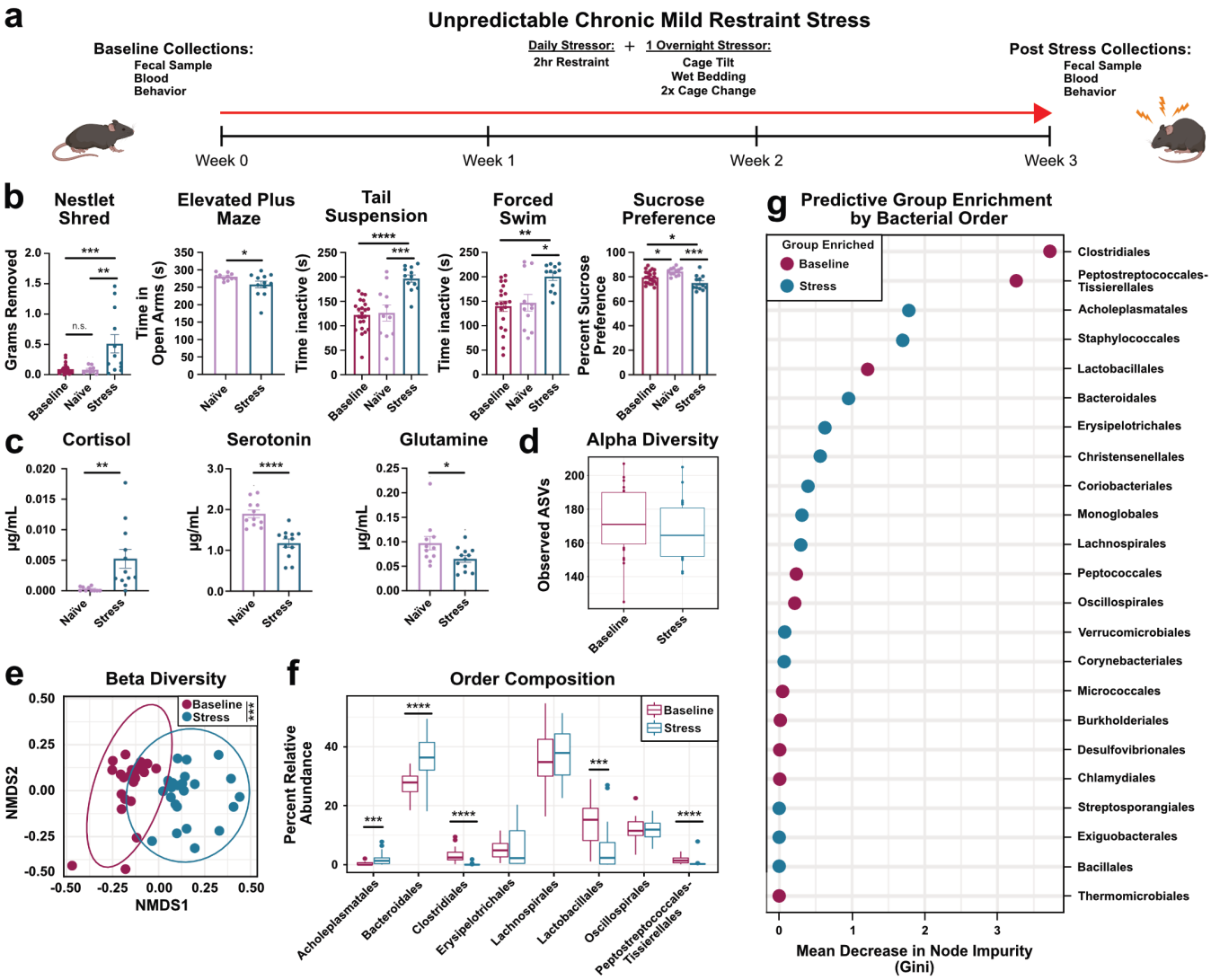

688

689 **Figure 1: Unpredictable Chronic Mild Restraint Stress Induces Anxiety and Depressive-like**

690 **Behaviors and Microbiome Dysbiosis:** (a) Experimental Design. (b) Nestlet shred (1WANOVA),

691 elevated plus maze (t-test), tail suspension (1WANOVA), forced swim (1WANOVA), and sucrose

692 preference (1WANOVA) tests between baseline, naïve controls, and stress animals. Male mice,

693 n=11/12 per group, N=2. (c) Mass spectrometry of serum of naïve or stress animals (t-tests). (d)

Alpha diversity plot showing microbial richness (observed ASVs) between baseline and stress mice (Wilcoxon Rank Sum test). (e) NMDS plot of Bray-Curtis dissimilarity between baseline and stress fecal microbiome samples (PERMANOVA). (f) Relative abundances of bacterial orders >1% (Wilcoxon Rank Sum test with Bonferroni correction). (g) Importance plot from a random forest model predicting bacterial orders that discriminate between baseline and stress groups. Importance is based on the Gini index, larger values are more important to model. Male mice, n=24/group, N=1.

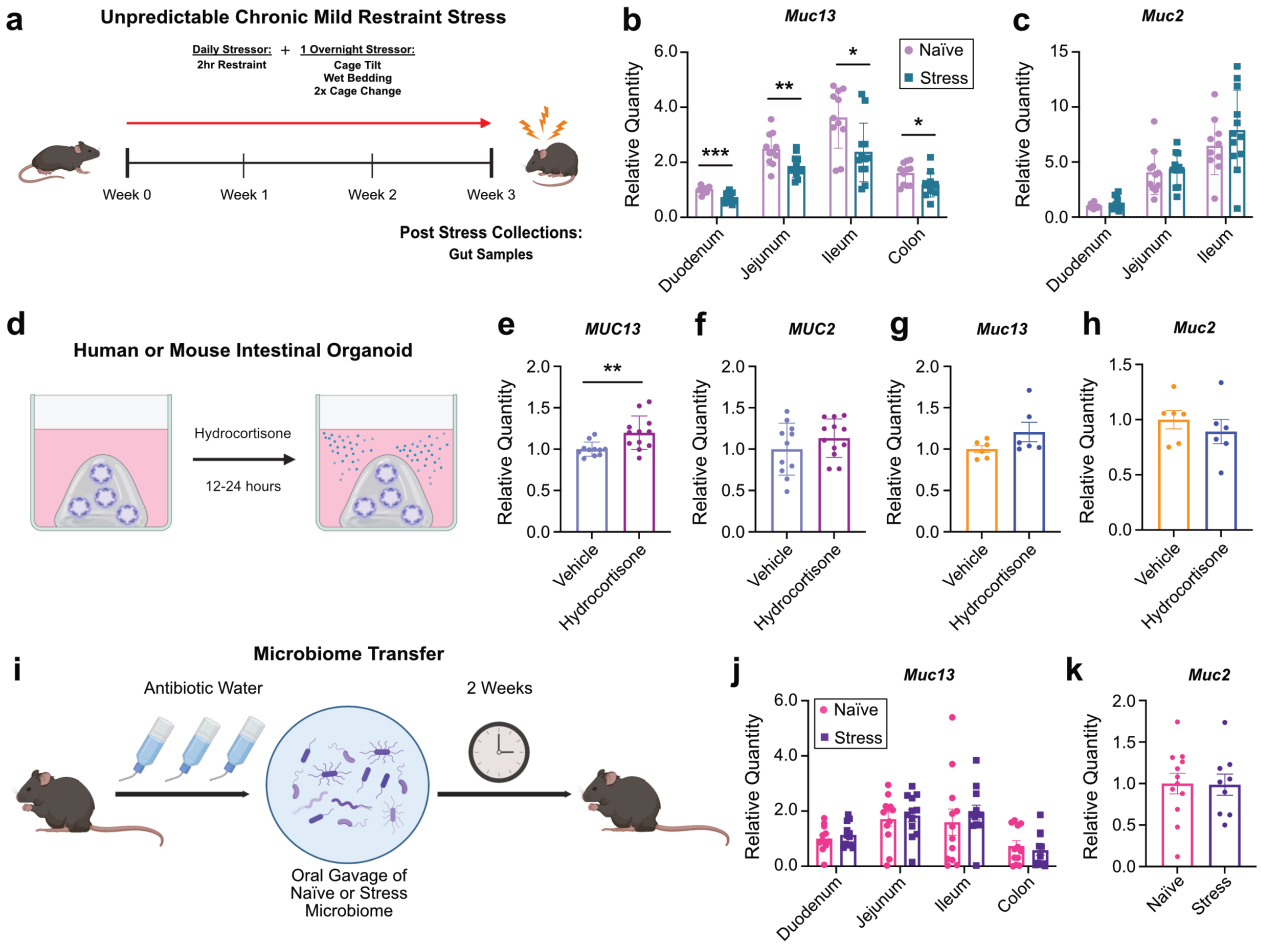

Figure 2: Reductions in Mucin 13 After Stress Exposure: (a) Experimental design. Relative quantity of (b) *Muc13* and (c) *Muc2* transcripts by qPCR in individual sections of the intestine. *Muc2* expression in the colon was higher than housekeeping genes preventing quantification by qPCR. 2WANOVA with Multiple Comparisons. Male mice, n=11/12 per group, N=2. (d) Experimental design. Relative quantity of (e) *MUC13* and (f) *MUC2* in human duodenal organoids treated with 200µM hydrocortisone for 12 hours. N=1, n=12 per group. T-tests. Relative quantity of (g) *Muc13* and (h) *Muc2* in mouse jejunal organoids treated for 24 hours with 5ng of hydrocortisone. N=1, n= 6 per group. T-tests. (i) Microbiome transfer experimental design. Relative quantities of (j) *Muc13* and (k) *Muc2* transcripts in the intestines of animals receiving a

712 naïve or stress fecal microbiome. Male mice, n=12 per group. *Muc2* only detected in the

713 duodenum. 2WANOVA with multiple comparisons (j) or t-test (k).

714

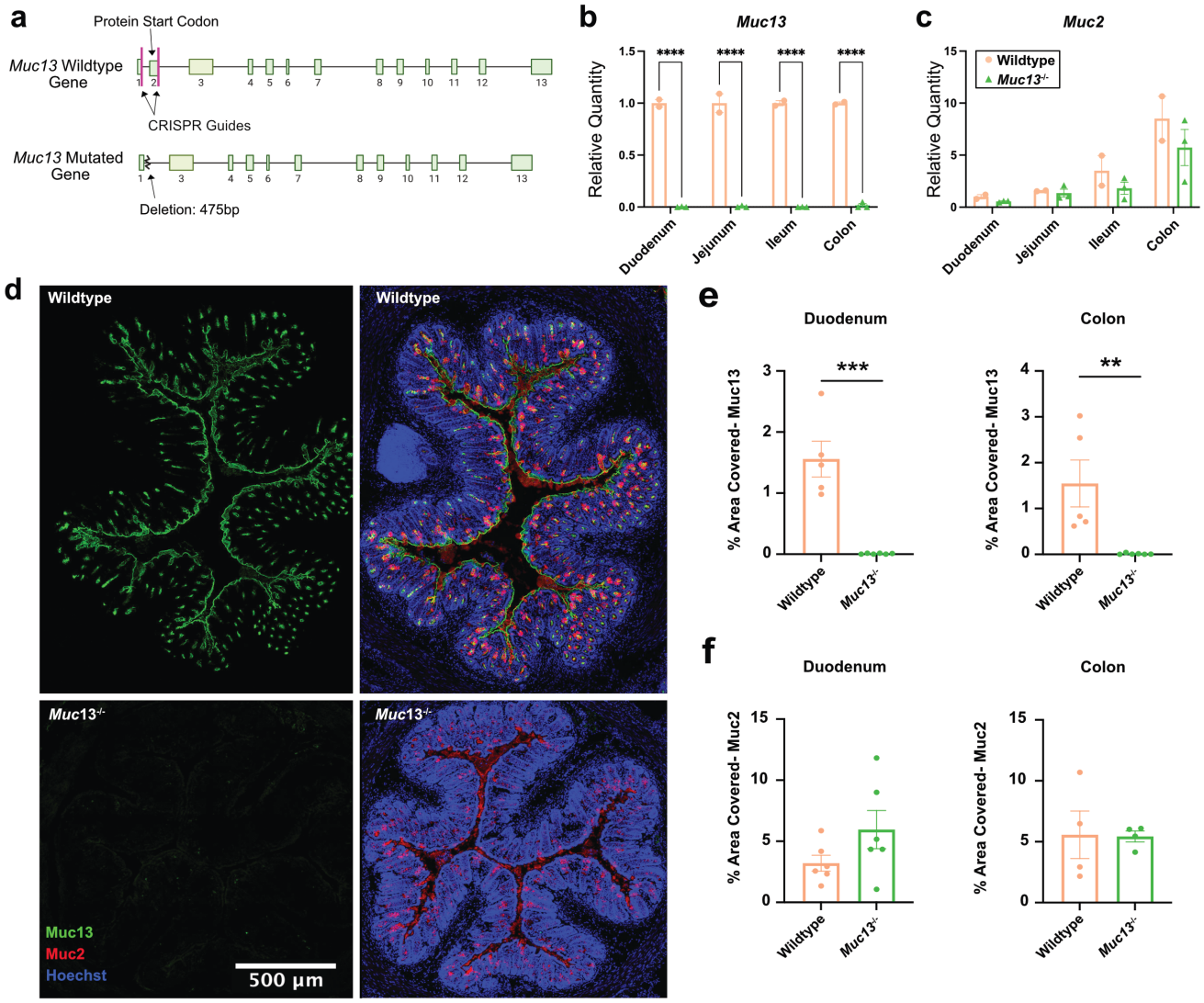

Figure 3: Mucin 13 Deletion Validation: (a) Strategy to inactivate mucin 13. Relative quantities of (b) *Muc13* and (c) *Muc2* in wildtype or *Muc13*$^{-/-}$ mice. Male mice, n=2-3 per group, N=1. 2WANOVA. (d) Representative images of immunofluorescence (IF) staining of Muc13, Muc2 and Hoechst in the colon of wildtype or *Muc13*$^{-/-}$ animals. Quantification of IF of (e) Muc13 and (f) Muc2 in the duodenum and colon of wildtype or *Muc13*$^{-/-}$ mice. Male mice. T-tests, n=4-6 per group, N=2.

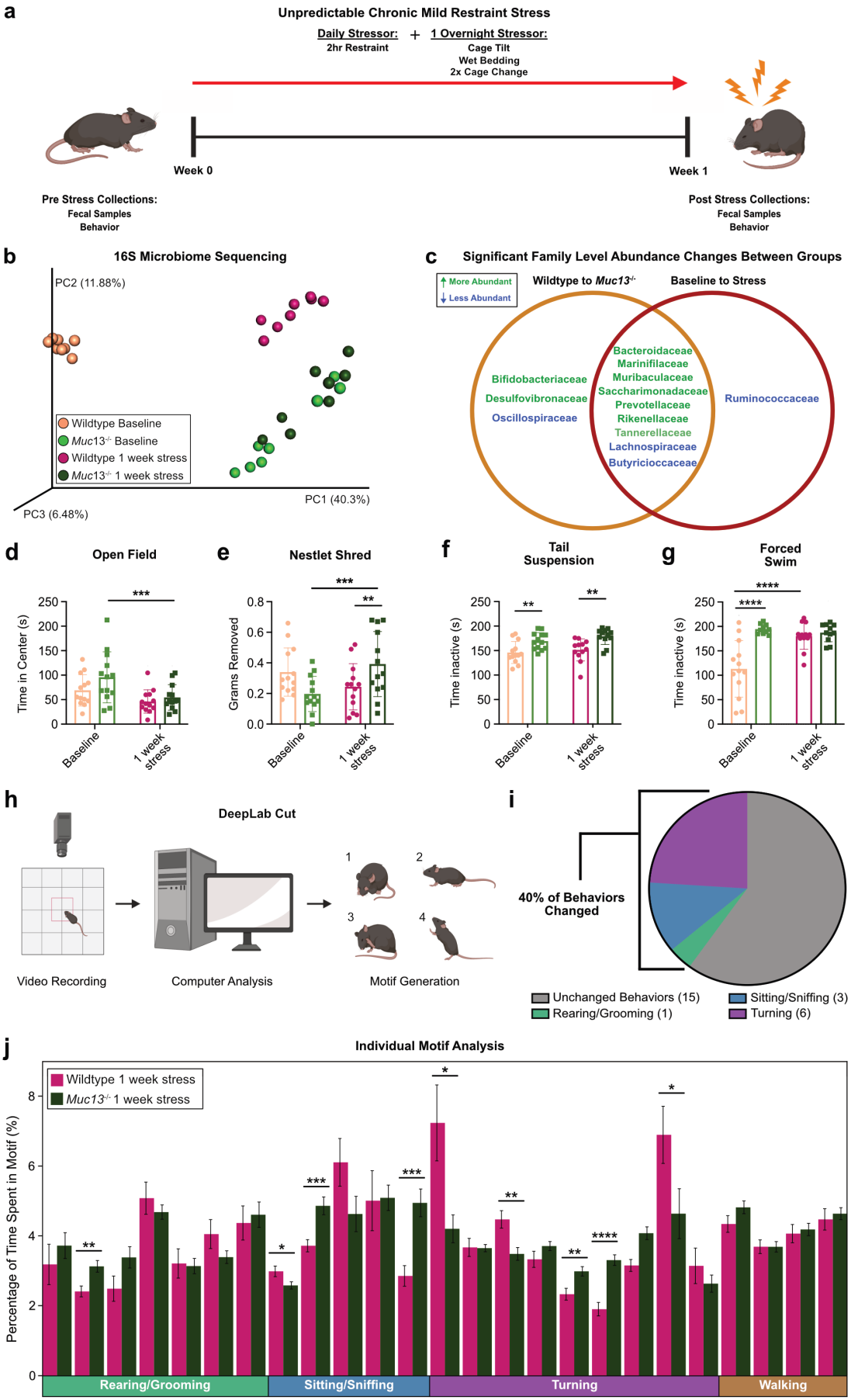
a
Unpredictable Chronic Mild Restraint Stress
Daily Stressor:
2hr Restraint
+
1 Overnight Stressor:
Cage Tilt
Wet Bedding
2x Cage Change
Week 0
Week 1
Pre Stress Collections:
Fecal Samples
Behavior
Post Stress Collections:
Fecal Samples
Behavior
b
16S Microbiome Sequencing
PC2 (11.88%)
PC1 (40.3%)
PC3 (6.48%)
Wildtype Baseline
Muc13-/- Baseline
Wildtype 1 week stress
Muc13-/- 1 week stress
c
Significant Family Level Abundance Changes Between Groups
More Abundant
Less Abundant
Wildtype to Muc13-/-
Baseline to Stress
Bifidobacteriaceae
Desulfovibronaceae
Oscillospiraceae
Bacteroidaceae
Marinifilaceae
Muribaculaceae
Saccharimonadaceae
Prevotellaceae
Rikenellaceae
Tannerellaceae
Lachnospiraceae
Butyricioccaceae
Ruminococcaceae
d
Open Field
Time in Center (s)
Baseline
1 week stress
e
Nestlet Shred
Grams Removed
f
Tail Suspension
Time inactive (s)
g
Forced Swim
Time inactive (s)
h
DeepLab Cut
Video Recording
Computer Analysis
Motif Generation
i
40% of Behaviors Changed
Unchanged Behaviors (15)
Sitting/Sniffing (3)
Rearing/Grooming (1)
Turning (6)
j
Individual Motif Analysis
Wildtype 1 week stress
Muc13-/- 1 week stress
Percentage of Time Spent in Motif (%)
Rearing/Grooming
Sitting/Sniffing
Turning
Walking

724 **Figure 4: Microbiome and Behavioral Changes in *Muc13*$^{-/-}$ Mice at Baseline and after Stress**
725 **Exposure:** (a) Experimental design. (b) PCoA plot of 16S fecal microbial sequencing in wildtype
726 and *Muc13*$^{-/-}$ animals at baseline and after 1 week of stress exposure. Male mice, n=8 per group,
727 N=1. (c) Venn diagram comparing significantly changed families from 16S fecal microbiome
728 sequencing between wildtype and *Muc13*$^{-/-}$ animals to families changes between wildtype
729 baseline and stress exposed animals. (d) Open field and (e) nestlet shredding tests comparing
730 anxiety-like behaviors between wildtype and *Muc13*$^{-/-}$ animals at baseline and after 1 week of
731 stress exposure. (f) Tail suspension and (g) forced swim tests between wildtype and *Muc13*$^{-/-}$
732 animals at baseline and after 1 week of stress exposure. Male mice, 2WANOVA, n=13 per group,
733 N=1. (h) DeepLabCut experimental design. (i) Pie chart of quantified behavioral motifs changed
734 between wildtype and *Muc13*$^{-/-}$ animals. (j) Individual motif analysis after 1 week of stress
735 exposure between wildtype and *Muc13*$^{-/-}$ animals. T tests, male and female mice, n=13-24 per
736 group, N=3.
737

738 **EXTENDED DATA**

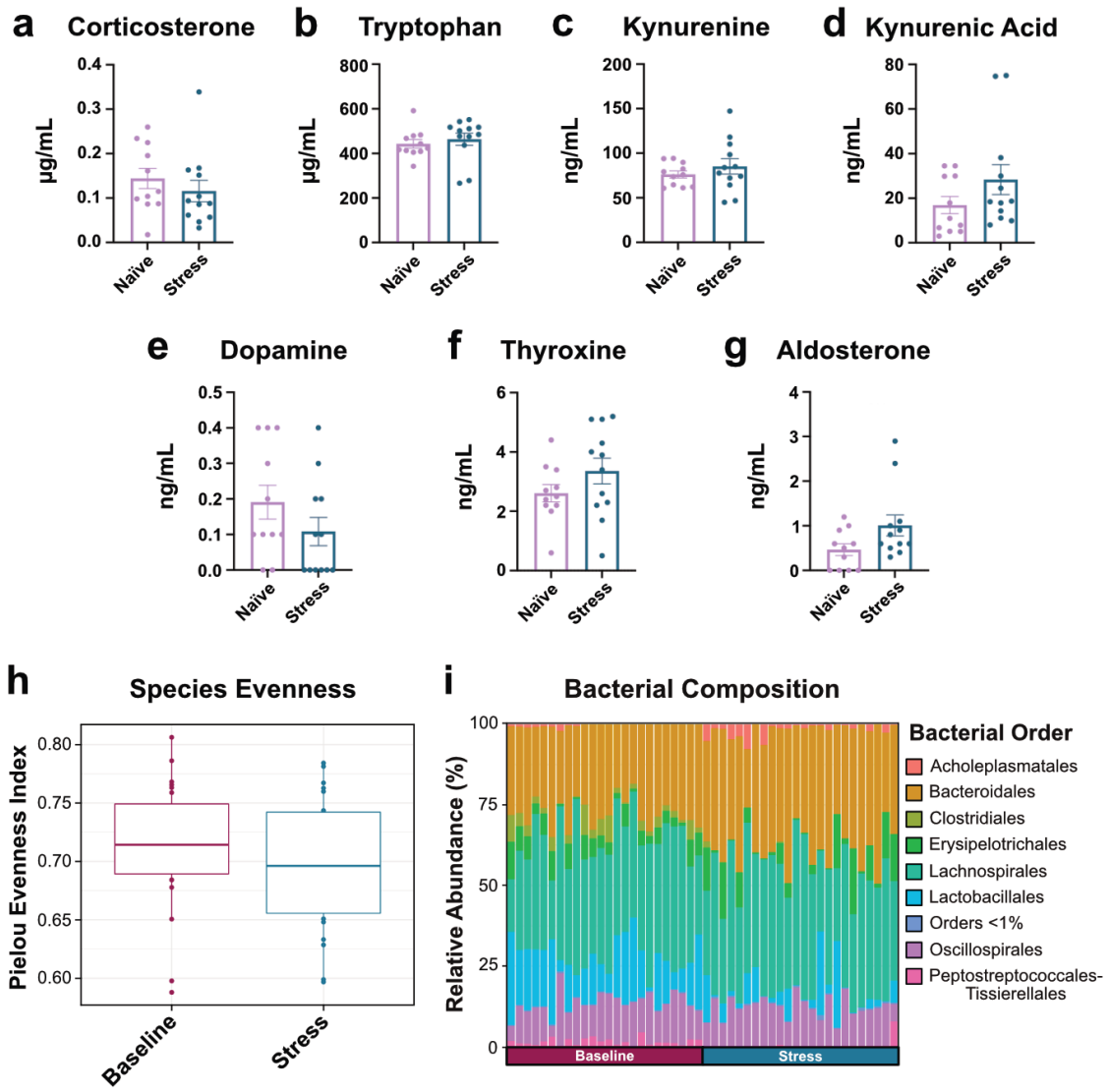

739

740 **Extended Data 1: Serum Metabolites and 16S Sequencing after Stress Exposure**: Mass

741 spectrometry analysis of serum from naïve or stressed mice. (a) corticosterone, (b) tryptophan,

742 (c) kynurenine, (d) kynurenic acid, (e) dopamine, (f) thyroxine, (g) aldosterone. Male mice,

743 n=11/12 per group, N=1. (h) Pielou's evenness index for baseline or stress mice. (i) Individual

744 order relative abundances for baseline or stress mice. Male mice, n=24/group, N=1.

745

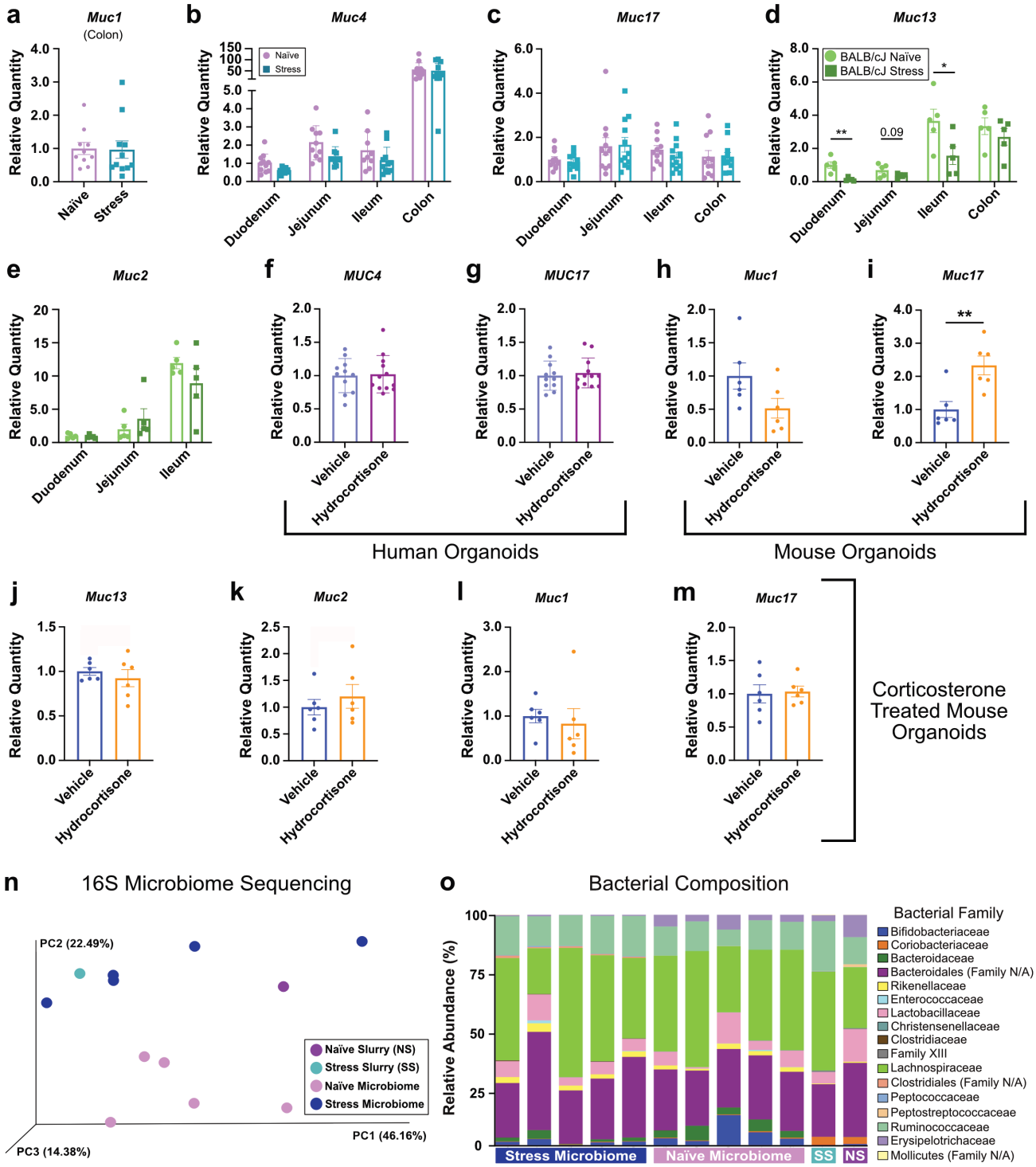
a
Muc1
(Colon)
Relative Quantity
Naïve
Stress
b
Muc4
Naïve
Stress
Duodenum
Jejunum
Ileum
Colon
c
Muc17
d
Muc13
BALB/cJ Naïve
BALB/cJ Stress
**
0.09
*
e
Muc2
f
MUC4
g
MUC17
h
Muc1
i
Muc17
Vehicle
Hydrocortisone
Human Organoids
Mouse Organoids
j
Muc13
k
Muc2
l
Muc1
m
Muc17
Corticosterone Treated Mouse Organoids
n
16S Microbiome Sequencing
PC2 (22.49%)
PC1 (46.16%)
PC3 (14.38%)
Naïve Slurry (NS)
Stress Slurry (SS)
Naïve Microbiome
Stress Microbiome
o
Bacterial Composition
Relative Abundance (%)
Bacterial Family
Bifidobacteriaceae
Coriobacteriaceae
Bacteroidaceae
Bacteroidales (Family N/A)
Rikenellaceae
Enterococcaceae
Lactobacillaceae
Christensenellaceae
Clostridiaceae
Family XIII
Lachnospiraceae
Clostridiales (Family N/A)
Peptococcaceae
Peptostreptococcaceae
Ruminococcaceae
Erysipelotrichaceae
Mollicutes (Family N/A)
Stress Microbiome
Naïve Microbiome
SS
NS

748 **Extended Data 2: Mucin Expression Changes and Mechanisms:** (a) Relative quantity of *Muc1*
749 expression in colon of naïve or stress mice by qPCR. *Muc*1 was not detected in other sections (t-
750 test). Relative quantities of (b) *Muc4* and (c) *Muc3/17* expression in the intestines of naïve or
751 stress mice by qPCR. (d) Relative quantity of *Muc13* and (e) *Muc2* expression in sections of the
752 intestines from naïve or stress BALB/cJ mice by qPCR. Multiple t-tests. Male mice. Experiments
753 a-c, n=11/12 per group. Experiments d-e, n=5 per group. N=1. Relative quantities of (f) *MUC4*
754 and (g) *MUC17* in human duodenal organoids treated with 200μM hydrocortisone for 12 hours.
755 N=1, n=12 per group. T-tests. Relative quantities of (h) *Muc1* (i) *Muc17* of mouse jejunal
756 organoids treated for 24 hours with 5ng of hydrocortisone. N=1, n= 6 wells per group. T-tests.
757 Relative quantities of (j) *Muc13*, (k) *Muc2*, (l) *Muc1*, and (m) *Muc17* in mouse jejunal organoids
758 treated for 24 hours with 150 μg of corticosterone. N=1, n= 6 wells per group. T-tests. (n) 16S
759 PCoA plot between naïve and stress slurries and naïve and stress microbiome recipients. (o)
760 Individual bacterial family compositions. Male mice, n=5/group, slurry samples from gavaged
761 microbiome mixture, N=1.
762

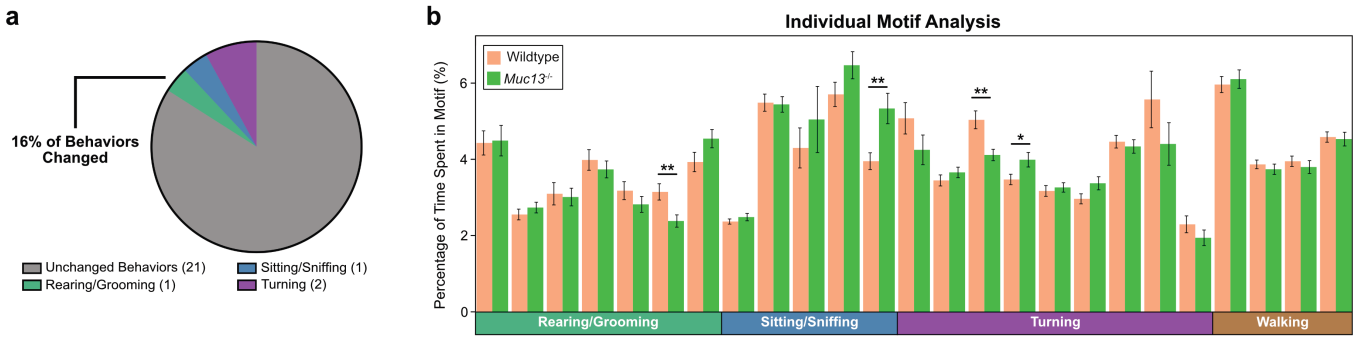

763

764 **Extended Data 3: DeepLabCut Analysis of Baseline Behaviors:** (a) Pie chart representing

765 quantified behavioral motifs changed between wildtype and *Muc13*$^{-/-}$ animals. (b) Individual

766 motif analysis comparing baseline behaviors in wildtype and *Muc13*$^{-/-}$ animals. T tests, male and

767 female mice, n=13-24 per group, representative of 3 experiments.

768

769

Analyte	Precursor m/z	Product m/z	RT
01_Dopamine	154.086	137.059	2.88
02_Norepinephrine	170.081	152.070	1.60
03_Serotonin	177.102	160.073	4.09
04_Kynurenic acid	190.050	162.055	8.05
05_Tryptophan	205.097	188.070	6.52
06_Kynurenin	209.092	94.065	4.73
07_Corticosterone	347.222	329.210	11.06
08_Aldosterone	361.201	343.189	10.80
09_Cortisol	363.217	327.194	10.93
10_Thyroxine	777.694	731.684	10.91
11_Glutamine	147.076	84.044	1.46

Extended Data 4: Mass Spectrometry Transitions: Table of mass over charge number (m/z) for analytes examined between naïve and stressed animals.

Target	Probe Product/Sequence Information
GAPDH	Taqman- Mm99999915_g1
Actin	Taqman- Mm02619580_g1
Muc1	Taqman- Mm00449604_m1
Muc2	Taqman- Mm01276696_m1
Muc3	Taqman- Mm01207064_m1
Muc4	Taqman- Mm00466866_m1
Muc13	Taqman- Mm00495397_m1
IL-4	Taqman- Mm00445259
IL-1B	Taqman- Mm00434228_m1
IL-33	Taqman- Mm00505403_m1
IFN-y	F: 5' TCTGAGACAATGACCGCTAC 3'
	R: 5' AGGCTTTCAATGACTGTGC 3'
Bmal	F: 5’ ACC AAC CCA TAC ACA GAA GC 3’
	R: 5’ GAC AGA CTC GGA GAC AAA GAG 3’
Rev-ERB alpha	F: 5’ GCC TCA TTT CTC CAT CAC CTA C 3’
	R: 5’ CGC AGT GAA GCA GGG TAA T 3’
Rev-ERB beta	F: 5’ CAC AGT GAG GGT TCT GAG AAT AG 3’
	R: 5’ CCG TTG GCA TCA CAG TTA GA 3’
Per1	F: 5' AGCTTTAGCCACGTGACAGTGA 3'
	R: 5' GGCAAGTGAAGAGGCCAACA 3'
Per2	F: 5’ AGAAAAGCCCTGCTGTTCCA 3’
	R: 5' CCAAATGCGGTGGTGTAGTTT 3'
Per 3	F: 5' GTGACAGCAGAGTCCCATGA 3'
	R: 5' CACTGCCATCTCGAGTTCAA 3'
MUC2	F: 5' CTGCTATGTCGAGGACACCC 3'
	R: 5' GAGTTGGTACACACGCAGGA 3'
MUC4	F: 5' CTTTTGTCCTCTTCCCAGGTTCC 3'
	R: 5' CAGTGTGAGGAGCAGACGTGA 3'
MUC13	F: 5' GGGAACTGCCAAAAGTGTGC 3'
	R: 5' CTGAGAATGACAATGCCAGCG 3'
MUC17	F: 5' GTTTCAACACCACTGGCACC 3'
	R: 5' CTGGTCCCGGTACTCCACTA 3'

Extended Data 5: qPCR Probes Used: A table of the qPCR probes used in the manuscript.